Insights into Photoinduced Sol–Gel Polymerization: An in Situ Infrared Spectroscopy Study

ARTICLE *in* THE JOURNAL OF PHYSICAL CHEMISTRY B · APRIL 2012

Impact Factor: 3.3 · DOI: 10.1021/jp212386e · Source: PubMed

5 AUTHORS, INCLUDING:

Heloise De Paz-Simon
Université de Haute-Alsace
10 PUBLICATIONS **43** CITATIONS
SEE PROFILE

Céline Croutxé-Barghorn
Université de Haute-Alsace
137 PUBLICATIONS **735** CITATIONS
SEE PROFILE

Didier Le Nouen
Université de Haute-Alsace
43 PUBLICATIONS **363** CITATIONS
SEE PROFILE

Séverinne Rigolet
Institut de Science des Matériaux de Mulhouse
85 PUBLICATIONS **764** CITATIONS
SEE PROFILE

THE JOURNAL OF PHYSICAL CHEMISTRY B

Article

pubs.acs.org/JPCB

Insights into Photoinduced Sol–Gel Polymerization: An *in Situ* Infrared Spectroscopy Study

Héloïse De Paz,[†] Abraham Chemtob,*[,†] Céline Croutxé-Barghorn,[†] Didier Le Nouen,[‡] and Séverinne Rigolet[§]

[†]Laboratory of Photochemistry and Macromolecular Engineering, University of Haute-Alsace, ENSCMu, 3, rue Alfred Werner, 68093 Mulhouse Cedex, France

[‡]Laboratory of Chemistry and Biochemistry, University of Haute-Alsace, ENSCMu, 3, rue Alfred Werner, 68093 Mulhouse Cedex, France

[§]Institute of Mulhouse Material Science, CNRS, LRC 7228, University of Haute-Alsace, 3 rue Alfred Werner 68093 Mulhouse Cedex, France

Supporting Information

ABSTRACT: Photoacid-catalyzed sol–gel polymerization is now recognized as a powerful single-step synthetic approach to the synthesis of hybrid films, which can be distinguished from conventional sol–gel methods by higher reactivity and a solvent-free process. Despite its utility, the mechanism is not yet understood, in particular what chemical, physical, and photochemical parameters determine the precise sequence, kinetics, and advancement of this UV inorganic photopolymerization. Here, using mainly transmission real-time Fourier transformed infrared (RT-FTIR) spectroscopy, we characterize *in situ* the hydrolysis–condensation reactions of oligomeric silicon alkoxides and the formation of byproducts. Systematic review and assessment of numerous processing variables (relative humidity, film thickness, precursor structure, nature, and the concentration of photoacid generator) prove that the reaction kinetics are controlled by the two independent phenomena: the intrinsic chemical reaction rates and the water vapor permeation into the film.

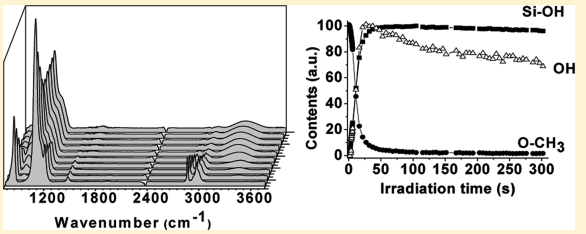

INTRODUCTION

As early as 1978, a patent from Fox et al.[1] proposed a photoacid-catalyzed sol–gel alternative to produce silica-based films in a single step and without the need for solvent. Conventional acid catalysts (acetic acid, HCl, HF, HNO_3) were replaced in the formulation by photoacid generators (PAG) such as diaryliodonium ($Ar_2–I^+$) or triarylsulfonium (Ar_3S^+) salts bearing weakly coordinating anions (X^-). The aromatic organic moiety of these salts ensures both an absorption in the range of 200–320 nm and solubility with the precursor to form a low-viscous and stable solution in absence of UV light, which can be deposited using the techniques described previously for polymeric sols. The UV irradiation causes a cascade of homolytic and heterolytic cleavages (Scheme 1) yielding protonic Brönsted superacids of the structure H^+X^-. The strongly delocalized charge on the anions (low electron pair donor ability) imparts a high catalytic reactivity to these protonic acids, originally widely used as initiators in the cationic photopolymerization of epoxy and vinyl ether organic monomers. The combination of fast PAG decomposition rate and superacidity induces a rapid solidification of the liquid precursor film, without apparent transition for a sol to a gel. Highly condensed films can be potentially achieved through appropriate choice and concentration of PAG, thus alleviating the constraint of thermal post-treatment and making such photoprocess suitable to thermally sensitive substrates.

Scheme 1. Mechanism of UV-Induced Photolysis of a Diaryliodonium Salt[a]

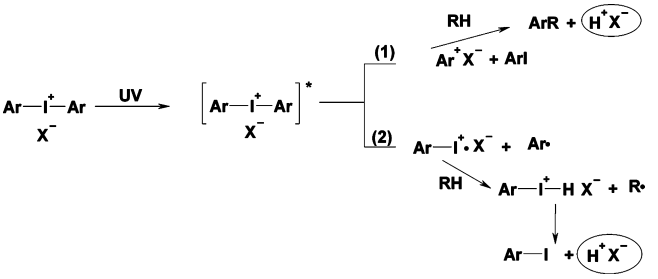

[a]Both heterolytic (1) and homolytic (2) reactions involving proton donors (RH) are responsible for the formation of superacids (H^+X^-).

The use of a photoinduced sol–gel process has already been reported in a few studies,[2−7] mainly in the design of novel one-step strategies toward nanocomposite films. In this paper, our goal is to discuss some fundamental aspects of photoinduced

Received: December 22, 2011
Revised: March 14, 2012

   dx.doi.org/10.1021/jp212386e | J. Phys. Chem. B XXXX, XXX, XXX–XXX

sol−gel processing, starting with simple alkoxysilane systems. As a silicon source, oligomeric precursors polydimethoxysiloxane (PDMOS) and polydiethoxysiloxane (PDEOS) were preferred to their monomeric analogues—tetramethoxysilane (TMOS) and tetraethoxysilane (TEOS)—to avoid evaporation problems. The fundamental questions surrounding photoacid-catalyzed hydrolysis and condensation in silicates concern what chemical, physical, and photochemical parameters determine the precise sequence, kinetics, and advancement of these reactions under different processing conditions. To the best of our knowledge, these issues have never been addressed as well as the major differences with a conventional sol−gel process. Here, we endeavor to discuss the influence of several experimental parameters such as film thickness, the relative humidity, the nature, and the concentration of PAG on the course of the sol−gel process.

An important part of our investigation lies on the *in situ* analysis of the sol−gel kinetics by real-time Fourier transformed infrared (RT-FTIR) spectroscopy. IR has been known for decades as a powerful routine characterization technique, which provides extensive information about optical, vibrational, chemical, and structural properties in sol−gel materials, in particular on films.[8−13] However, the systematic presence of solvent saturating the signal and the weak reactivity inherent in a conventional sol−gel polymerization makes the implementation of a rapid scan time-resolved FTIR either incompatible or useless. Therefore, the use of RT-FTIR concerned only periodically organized silica films after the deposition stage with a main emphasis on solvent evaporation and silica network condensation.[14−16] The implementation of a solvent-free and fast photo sol−gel process opens new opportunities for RT-FTIR, with the possibility to investigate structural aspects but also reaction kinetics and the formation of byproducts, without affecting the course of the polymerization.

EXPERIMENTAL SECTION

Chemicals. Polydimethoxysiloxane (PDMOS) and polydiethoxysiloxane (PDEOS) were purchased from ABCR and used without further purification. PDMOS and PDEOS are nonhydrolyzed oligomeric silicate precursors derived respectively from tetramethoxysilane (TMOS) and tetraethoxysilane (TEOS). PDMOS, also called methyl silicate, is a cheaper source of silicon than TMOS. It results when TMOS is synthesized in presence of traces of water and HCl byproduct. In practice, reaction conditions are chosen that give on ignition SiO_2 equivalent to 51 wt % for PDMOS and 40% for PDEOS, which corresponds to an average of five silicon atoms per oligomer. Significant differences in silicate speciation were observed depending on the alkoxy group. Liquid state ^{29}Si NMR of the PDMOS oligomer precursor exhibits four signals attributed to Q^0 (Si-$(OR)_4$, 1.8%), Q^1 ($(RO)_3$-Si-(OSi), 49.7%), Q^2 ($(RO)_2$-Si-$(OSi)_2$, 44.4%), and Q^3 ((RO)-Si-$(OSi)_3$ 4.1%) and for the PDEOS Q^0 (Si-$(OR)_4$, 7.9%), Q^1 ($(RO)_3$-Si-(OSi), 33.7%), Q^2 ($(RO)_2$-Si-$(OSi)_2$, 42.8%), and Q^3 ((RO)-Si-$(OSi)_3$, 16.4%). In reality, PDMOS and PDEOS consist of a mixture of linear, branched, and cyclic structures. The coupling of different liquid state NMR techniques (^{29}Si, ^{13}C, ^{1}H) was essential to shed light onto the structure of the alkoxy oligomers (Figures S1 and S2, see Supporting Information for complete discussion). The photoacid generators diphenyliodonium hexafluorophosphate ($\Phi_2I^+PF_6^-$), diphenyliodonium triflate ($\Phi_2I^+CF_3SO_3^-$), diphenyliodonium toluenesulfonate ($\Phi_2I^+CH_3\Phi SO_3^-$), and diphenyliodonium chloride ($\Phi_2I^+Cl^-$) were purchased from Sigma-Aldrich and used as received.

Silica Film Preparation. In a typical procedure, 2 wt % of PAG ($\Phi_2I^+PF_6^-$) was dissolved in the inorganic precursors (PDMOS or PDEOS) to form a photolatent solution in the absence of UV light. Then, the resulting formulation was deposited on a BaF_2 pellet using a spin-coater (Delta 6TT by SÜSS Microtech) at a 2000 rpm speed for 50 s to produce a 0.9 ± 0.2 μm and a 1.9 ± 0.5 μm liquid film layer for respectively PDMOS and PDEOS. Irradiation was performed at room temperature under a UV irradiation device implemented for RT-FTIR, in which formulations were simultaneously exposed to UV light and to an IR analytical beam. During UV irradiation, the relative humidity[17] (RH) was maintained between 27 and 33%. All measurements were performed in an environmental cell. The relative humidity was controlled by using saturated solutions of salt such as NaCl or MgCl. Films were irradiated subsequently by the polychromatic light of a mercury−xenon lamp (Hamamatsu, L8251, 200 W fitted with a 365 or 254 nm reflector) and coupled with a flexible light guide, with an incident exitance of 200 mW/cm^2. The end of the optical guide was placed at a distance of 3 cm from the film and directed at an incident angle of 90° onto the sample window. After a 1 h irradiation, an increase of temperature of only 4 °C was measured, which has a limited impact on the photosolgel proccess. All measurements were repeated at least three times, and reproducible results were obtained.

In addition, a second UV irradiation system was used for the synthesis of samples devoted to ^{29}Si solid-state NMR spectroscopy, which requires a greater amount of product for the analysis (200−300 mg of the scratched film). In this case, the films were prepared on glass substrates and photopolymerized under a UV conveyor with a belt speed of 10 m/min using a microwave lamp (H lamp, Fusion) and an exitance of 1.46 J/cm^2 per pass. The samples were subjected to five successive passes under the conveyor to yield transparent solid film. During the UV irradiation, the room humidity was maintained between 30 and 35% with a hygrometer.

Characterization. Infrared spectra obtained by RT-FTIR were recorded in transmission with a Bruker Vertex 70 spectrophotometer equipped with a liquid-nitrogen-cooled mercury−cadmium telluride (MCT) detector. The resolution of the infrared spectra was 4 cm^{-1}. During the UV irradiation, the absorbance decrease of the CH_3 symmetric stretching vibration band centered at 2848 cm^{-1} was monitored to follow the methoxysilyl hydrolysis in PDMOS, while its analogue at 2890 cm^{-1} was used for PDEOS. All spectra were baseline corrected prior to integration with the software OPUS 6.5. The linear part of the evolution of hydrolysis conversion versus reaction time allowed the determination of initial rates of hydrolysis (r_p, (L mol^{-1} s^{-1})) and the calculation of the corresponding $r_p/[PDMOS]_0$ values (s^{-1}), $[PDMOS]_0$ representing the initial precursor concentration. Relative rates of hydrolysis (eq 1) could be calculated, taking the initial rate of hydrolysis with a film thickness of 0.9 μm (1.9 μm with PDEOS), a RH of 30%, and a PAG concentration of 2 wt % and under maximum polychromatic exitance (200 mW/cm^2) as a reference.

$$r_p^{rel} = \frac{r_p([PAG], RH, exitance, thickness)}{r_p(ref)} \quad (1)$$

dx.doi.org/10.1021/jp212386e | J. Phys. Chem. B XXXX, XXX, XXX−XXX

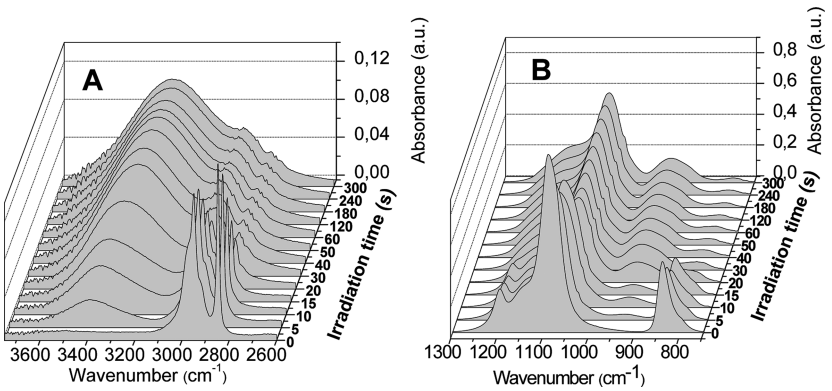

Figure 1. *In situ* time-resolved FTIR spectra on a time scale of 300 s of a PDMOS film containing 2 wt % of PAG under UV irradiation in the range of 3750−2600 cm^{-1} (A) and 1300−700 cm^{-1} (B).

Films thicknesses were assessed by profilometry using an Altisurf 500 workstation (Altimet) equipped with a 350 μm AltiProbe optical sensor for liquid films and a microforce sensor for solid films. Solution state NMR spectra were obtained using a Bruker Avance spectrometer equipped with a Bruker broadband BBI 5 mm probe. The spectra were acquired at 79.49 MHz for ^{29}Si nuclei. The solution state ^{29}Si spectra of the polysiloxanes were obtained in $CDCl_3$ solution (30 vol %) without proton decoupling. Tetrametylsilane (TMS) was used as internal reference. A recycled delay of 20 s is sufficient for full spin relaxation, and the spectra were acquired for 12 h at room temperature using a $\pi/3$ pulse with a pulse time of 15 μs. To obtain quantitatively reliable ^{29}Si solid state NMR spectra of the UV-cured films, single pulse magic angle spinning (SPE-MAS) experiments were performed on a Bruker Avance II 300 spectrometer operating at B_0 = 7.2 T (Larmor frequency: υ_0(Si) = 59.6 MHz) with a Bruker double channel 7 mm probe. The spectra were recorded using a pulse angle of $\pi/6$, a recycling delay of 80 s, a spinning frequency of 4 kHz, and high-power proton decoupling during the acquisition. These recording conditions ensured the quantitative determination of the proportions of the different Q^n siloxane species in photopolymerized PDMOS and PDEOS. All MAS NMR experiments were performed at room temperature, and chemical shifts reported thereafter are relative to tetramethylsilane. Deconvolution of the spectrum was performed using Dmfit software.[18]

RESULTS AND DISCUSSION

RT-FTIR Study of Sol−Gel Photopolymerization: Hydrolysis, Condensation and Sol−Gel Byproducts. The IR spectra of a PDMOS film (0.9 μm) containing 2 wt % of PAG ($\Phi_2I^+PF_6^-$) were recorded with a maximum time resolution of 0.12 s following UV irradiation. *In situ* time-resolved spectra on a time scale of 300 s were shown as three-dimensional plots in Figures 1A (3750−2600 cm^{-1}) and 1B (1300−700 cm^{-1}), with the wavenumber in the *x*-axis and the irradiation time in the *y*-axis. The first region encompasses mainly the OH (3400 cm^{-1}) and OCH_3 (~2900 cm^{-1}) stretching modes involved in the hydrolysis stage while the second is more informative of polycondensation reactions through the Si−O−Si (1100 cm^{-1}) and Si−OH (930 cm^{-1}) stretching modes. Before reaction (t = 0 s), a broad band around 1100 cm^{-1} is already visible in PDMOS as expected from its oligomeric structure, while the absence of any OH signal confirms the absence of hydrolyzed products. Speciation of silicate condensates in PDMOS and PDEOS precursors was thoroughly discussed in the Supporting Information from their ^{29}Si NMR spectra (Figures S1 and S2). Compared with a traditional method of preparing sol−gel silicate films, two differences should be particularly emphasized: namely, the absence of reaction without UV light (photolatency) and a steady film thickness after deposition due to a solvent-free formulation. As a corollary, a complete picture of the hydrolysis and condensation kinetics can be contemplated based on the results of RT-FTIR investigations. In the following sections, three distinct and concomitant processes were investigated: hydrolysis, polycondensation, and the development of sol−gel byproducts (water, alcohol). Reactions kinetics were systematically related to the mechanisms and the chemistry occurring at the short-length scale to gain insight into the driving forces controlling the structural evolution in silicate systems under UV irradiation. The assignments of the main IR bands of PDMOS are gathered in Table 1.

Table 1. Main Infrared Absorption Bands of PDMOS

wavenumber (cm^{-1})	assignment	wavenumber (cm^{-1})	assignment
~3740	υ OH (free) (stretching)	~1100	ν_{asym} Si−O−Si
~3400	υ OH (hydrogen bonded)	1090	ν_{asym} C−O
2950	ν_{asym} CH_3	930	υ Si−O^-, υ Si−OH
2848	ν_{sym} CH_3	839	ν_{sym}C−O
1640	δ H_2O (bending)	793	ν_{sym} Si−O−Si
1458	δ_{asym} CH_3	460	ρ Si−O−Si
1196	ρ CH_3 (rocking)		

Hydrolysis. As displayed in Figures 1A and 1B, a fast decrease in intensity of the stretching bands at 839 (ν_{sym} (C−O)), 1090 (ν_{asym} (C−O)), 2950 (ν_{asym}(CH_3)), and 2848 cm^{-1} (ν_{sym} (CH_3)) follows the irradiation of the PDMOS film, translating the progressive hydrolysis of the methoxy functions during the irradiation. Interestingly, the latter symmetric CH_3 stretching vibration appears as a sharp isolated band, making it well-suited for a temporal analysis of the hydrolysis kinetics. In contrast, the neighboring out-of-phase asymmetrical CH_3 vibration at 2950 cm^{-1} is significantly broadened by methyl deformation overtones, which belong to the same symmetry species as the symmetrical CH_3 and are probably involved in Fermi resonances interactions with the in-phase CH_3 stretch vibration. Systematic deconvolution and integration of the

dx.doi.org/10.1021/jp212386e | J. Phys. Chem. B XXXX, XXX, XXX−XXX

strong band at 2848 cm^{-1} at the low end of the CH_3 region gave a unique insight into the fast hydrolysis conversion−time curve (Figure 2A). Note that similar kinetic profiles were

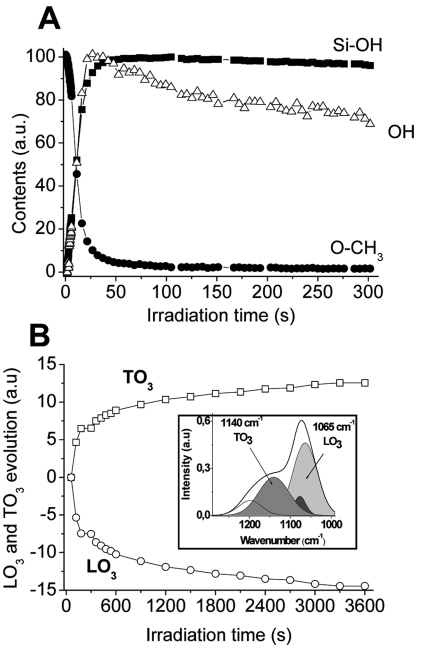

Figure 2. Area evolution (integrated absorbance) of the FTIR bands: O−CH_3 (●, $\nu_{asym}(CH_3)$, 2848 cm^{-1}), OH (△, ν(OH), 3400 cm^{-1}), and Si−OH (■, υ(Si−O), 930 cm^{-1}) during the UV irradiation of a PDMOS film (A). Relative evolution of TO_3 (□) and LO_3 (○) Si−O−Si asymmetric stretching modes during the irradiation time. The insert is a deconvolution of the FTIR absorption spectrum in the 1000−1300 cm^{-1} interval (B).

obtained when integrating less intense CH_3 vibrational bands such as the symmetrical CH_3 deformation band at 1458 cm^{-1} (not represented) or the CH_3 rocking at 1196 cm^{-1} (Figure 1B). As represented in Figure 2A, only 11 s was necessary to consume half the methoxysilyl functions. Second, a slowdown happens, and 50 s of irradiation was eventually required to reach almost a full hydrolysis, which is an indirect indication of concomitant condensation reactions affecting the course of the hydrolysis in a more constraint silicate environment. Under most conditions in conventional sol−gel chemistry, condensation is known to commence before hydrolysis is complete.

Hydrolysis is also manifested by the formation of Si−OH groups, which absorb like the alcohols at 3700−3200 cm^{-1} owing to the stretching of the OH−O bonds (Figure 1A). Such a band actually encompasses the contribution of all hydroxyl-containing compounds: silanol and possibly methanol and water byproducts. Even after 5 s irradiation, the OH stretching band is centered at 3400 cm^{-1}, suggesting the formation of a majority of hydrogen-bonded OH groups, with almost no contribution from free surface silanols (3740 cm^{-1}). As shown in Figure 2A, a complete correspondence between methoxy moieties disappearance and the OH band growth during the hydrolysis stage is observed, which is in agreement with the direct conversion of Si−$OCHH_3$ into Si−OH. More specific of silanol is a strong band due to Si−O stretching vibrations occurring at 930 cm^{-1}, whose evolution coincides also precisely with that of the alkoxide groups.

Condensation. During the hydrolysis, the Si−O−Si antisymmetric stretching band in the region 1000−1260 cm^{-1} is not resolved from the presence of the strong ν_{asym} (Si−)O−C band (1090 cm^{-1}).[19] Nevertheless, the completion of hydrolysis after 50 s makes this region uniquely representative of the silica network and therefore exploitable to investigate the progress of condensation. We recognize in Figure 1B the signature of the IR spectrum of pure silica at the end of hydrolysis with a band centered at ∼1065 cm^{-1} related to longitudinal optical mode (LO_3) of the antisymmetric stretching accompanied by a clearly visible shoulder at ∼1140 cm^{-1} associated with the transverse optical mode (TO_3) of the same vibration. Following the assignment proposed by Fidalgo et al.,[12] the broad envelope was deconvoluted into four Gaussians (inset of Figure 2B): two major bands at 1065 (LO_3) and 1140 cm^{-1} (TO_3) with two minor components at 1075 and 1205 cm^{-1}. These latter bands were attributed to equivalent modes, but of different structural units (4-fold ring), and will not be discussed. The evolution of the relative areas underlying the two dominant bands was estimated throughout a longer irradiation time of 3600 s. As seen graphically in Figure 2B, a slight increase in area of the TO component was accompanied by a decrease of that of LO. Similar evolution has already been reported by Innocenzi et al.[13] upon thermal treatment and interpreted as the sign of the formation of additional siloxane bonds or perhaps siloxane bond orientation. Thus, the general trend supports a condensation occurring not only in a concomitant way with hydrolysis but also subsequently.

There are two other signs in line with the previous conclusion of a continued condensation after hydrolysis (t > 50 s): a sharp decrease in the area of the OH band at 3400 cm^{-1} as well as a slight reduction of the Si−OH band at 930 cm^{-1}, both evaluated in Figure 2A. In accordance with these results, the photoacid-catalyzed sol−gel mechanism would proceed in two consecutive stages comprising a first part in which fast hydrolysis and condensation reactions take place concurrently (t < 50 s) followed by a single and slow condensation step (t > 50 s). Regarding the overall sol−gel mechanism, one must point out that the substitution of methoxy groups for ethoxy groups (Figure 3) does not change

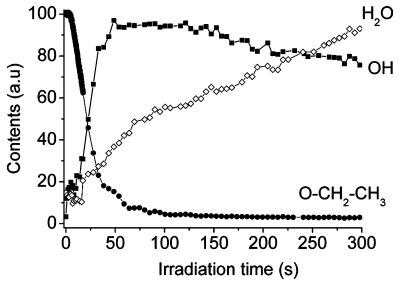

Figure 3. Temporal evolution of the integrated absorbance of the FTIR bands: O−CH_2CH_3 (●, $\nu_{asym}(CH_3)$, 2890 cm^{-1}), OH (■, ν(OH), 3400 cm^{-1}) and H_2O (◇, $\delta(H_2O)$, 1640 cm^{-1}) during the UV photopolymerization of a PDEOS-based film.

the general trends shown in Figure 2A in the case of PDMOS. The main difference is that the hydrolysis rate of PDEOS is significantly lowered, leading to retardation to obtain a full consumption, as expected from the alkoxy group hindrance effect reported in conventional sol−gel chemistry.[20,21] Thus, a consistent trend is apparent whatever the alkoxide substituent.

A better overview of the siloxy microstructure was also given by solid-state ^{29}Si CP SPE NMR. Figure 4 displays the quantitative spectrum of UV cross-linked PDMOS and PDEOS

dx.doi.org/10.1021/jp212386e | J. Phys. Chem. B XXXX, XXX, XXX−XXX

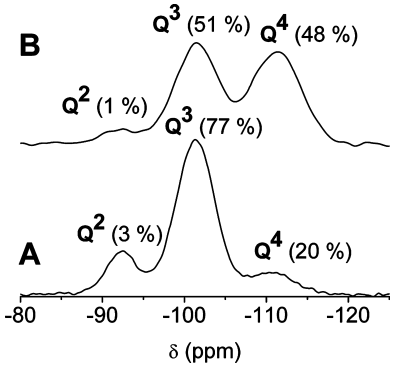

Figure 4. Solid-state ^{29}Si CP SPE MAS NMR spectra of UV cross-linked PDEOS (A) and PDMOS (B) films. Irradiation conditions: UV conveyor, H lamp, 1.46 J/(cm^2 pass), 5 passes.

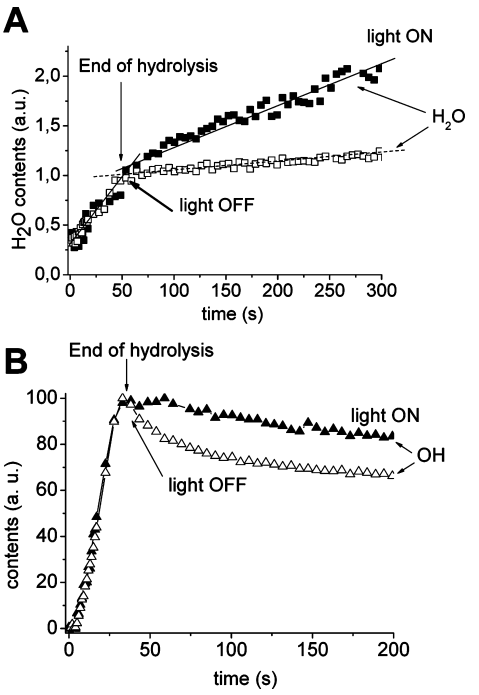

Figure 5. Variation in water content (A) and in hydroxyl functions (B) in a UV-irradiated PDMOS film determined from the integrated absorbance of the FTIR bands at 1640 cm^{-1} (δH_2O) and 3400 cm^{-1} (νOH), respectively. Full symbols indicate a continuous irradiation while open symbols correspond to a 50 s irradiation (a time corresponding to the end of hydrolysis).

films dominated by Q^3 ((HO)Si(OSi)$_3$, ~−95 ppm) and Q^4 (Si(OSi)$_4$, ~−110 ppm) siloxane species, indicating that the photoinduced sol−gel process leads to well-condensed materials. The characterization of the siloxane subspecies was determined by resonance ratios deconvolution and integration of the solid-state ^{29}Si NMR spectrum. As reported in conventional sol−gel chemistry, higher condensation degrees were found for PDMOS (87%) compared to PDEOS (78%). For solid-state NMR analysis with low-abundance nucleus such as ^{29}Si, a much higher quantity of product was required than the amount produced during the RT-FTIR experiment. Consequently, the silica films for solid-state NMR were synthesized under a UV conveyor, keeping all other experimental parameters unchanged.

Sol−Gel Byproducts: Water and Methanol. Obviously, excess water is not necessary for hydrolysis, which is a remarkable feature since additional water would have required the use of cosolvents to ensure miscibility with the inorganic precursor. However, the reaction mechanism remains definitively hydrolytic but with a hydrolysis stage fed by the continuous flux of atmospheric moisture diffusing into the sample. The presence of water dissolved in PDMOS initially was evidenced by its bending mode at 1640 cm^{-1}, whose area was assessed continuously throughout the irradiation as represented in Figure 5A. Despite the relative hydrophobicity of the methoxy oligomeric precursor, water is already apparent in the IR spectrum of PDMOS before reaction (t = 0 s). Contrary to what has been expected, the hydrolysis stage is marked by a progressive enrichment in water. This apparent contradiction may be explained in part by enhanced film hydrophilicity as a result of the replacement of alkoxide groups by hydroxyl groups, thereby increasing the water adsorption ability.[15] A second and important factor is the water generated as a byproduct of the condensation (occurring concomitantly with hydrolysis). Entrapment of water molecules may be also favored by virtue of hydrogen bonding with silanol groups and the formation of a solid oxo-polymer network. A more detailed observation of the water content (Figure 5A) actually reveals a two-step regime in water uptake: a fast linear increase with the irradiation time that declines substantially after the end of hydrolysis. This is consistent with a change in water vapor permeation after hydrolysis, which will be discussed in finer detail in the next section.

Unlike water, methanol byproduct is not manifested by a distinctive vibrational band in the IR spectrum. The O−H stretching vibration in the 3800−2800 cm^{-1} region actually includes the contribution of all hydroxyl-containing species, making the precise identification of alcohol tedious. However, evaporation of methanol could be evidenced indirectly by observing the downward evolution of OH stretching band at the end of hydrolysis (t > 50 s, Figure 5B). Compared to a film under continuous irradiation, stopping the UV light after hydrolysis caused surprisingly a faster decrease in the OH band. Given that condensation is significantly slowed after the UV shutdown, it appears justified to relate this decrease to the progressive desorption of volatile methanol. Under continuous irradiation, methanol evaporation still takes place (as well as further silanol condensation), but the loss of hydroxyl containing compounds is partially offset by a significantly enhanced formation of water, as displayed in Figure 5A, leading to a slower decline of the OH band. A limited methanol concentration in the film is particularly relevant in view of the secondary effects of alcohol in sol−gel chemistry. Alcohols are indeed not inert solvents as they are known to promote reesterification (reverse process of hydrolysis) and depolymerization reactions. According to Le Châtelier's principle, the system should respond to the elimination of methanol by increasing the forward reaction rates consuming the methoxysilyl groups. As a result of alcohol evaporation, the position of the hydrolysis "equilibrium" is thus shifted to the right, which may account for the fast hydrolysis rates found in this system.

The residual presence of methanol and water byproduct was also investigated in the final material through ^{1}H MAS NMR spectroscopy (Figure 6).

The high field region is rather characteristic of silanol groups with two signals at 1.1 and 2.3 ppm assigned respectively to vicinal (Q^3) and germinal (Q^2) Si−OH, whose relative intensity is consistent with the ^{29}Si NMR spectrum (Figure

dx.doi.org/10.1021/jp212386e | J. Phys. Chem. B XXXX, XXX, XXX−XXX

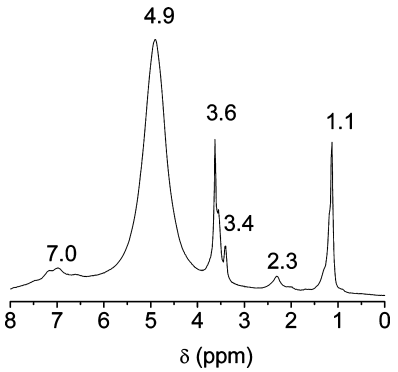

Figure 6. ^{1}H MAS NMR spectrum of UV cross-linked PDMOS film.

4). [22] The existence of water is exemplified by at least two resonances: a large signal at 4.9 ppm (liquidlike physisorbed water) and a broad shoulder at 7 ppm (strongly hydrogen-bonded water). [23] Of interest is also the distinct double maximum signal around 3.5 ppm. An assignment to less hydrogen-bonded water molecules can be tentatively considered at this chemical shift, but this multimodal resonance may also mirror the presence of methanol trapped in the oxo-polymer network. The maxima at 3.4 and 3.6 ppm are fully consistent with the methyl and hydroxyl groups of methanol, respectively.

Driving Force of the Photoinduced Sol–Gel Process. There is another question which begs to be answered in regard to the driving forces of the hydrolysis–condensation reactions. It has been well established that Brönsted photoacids can act as efficient photocatalysts of the sol–gel polymerization, with a mechanism presumably similar to that described in conventional acid-catalyzed sol–gel process. [24] In addition, we considered the possibility that the electronic excitation promoted by energetic UV photons might promote a densification of the inorganic network. In order to assess the relevance of this hypothesis, we focused on the condensation reactions occurring after the hydrolysis stage (t > 50 s).

Upon using a 254 nm reflector instead of 365 nm reflector (used in all the previous experiments), a higher amount of photons below 300 nm can be produced by the same Hg–Xe lamp (see Figure S3 for the emission spectra with the two reflectors). As shown in Figure 7A, this change caused a faster decrease of the band assigned to silanol (930 cm^{-1}) and OH groups (3400 cm^{-1}).

Accordingly, the evolution of the LO_3 and TO_3 components of the broad envelope in the 1000–1260 cm^{-1} was significantly enhanced using the 254 nm reflector as displayed in Figure 7B. Both results agree for a substantial acceleration of the condensation process, making clear that energetic photon UV can directly induce a silica densification, in addition to a photoacid-catalyzed condensation. Note that irradiation raised the substrate temperature by less than 40 °C. Thus, the structural changes in silica films are assumed to be mainly ascribed to electronic processes stimulated by irradiation. The concept of UV photoinduced densification of sol–gel derived metal oxide films (SiO_2, TiO_2) has been already reported in the literature, mostly with energetic UV light source such as low-pressure mercury lamps (254 nm) [25] and excimer lamps (172 nm). [26,27] Imai et al. [28] suggested that energetic enough photons can stimulate the electronic excitation of silanol groups and Si–O–Si bonds to induce silanol condensation and the structural rearrangement of the silica network. In our case, the ongoing

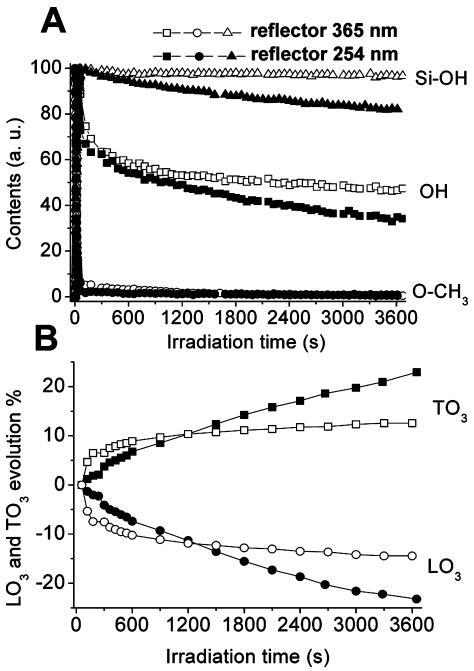

Figure 7. Evolution of the O–CH_3 (●, ○), OH (■, □), and Si–OH (▲, △) FTIR bands during the UV irradiation of a PDMOS film with a Hg–Xe lamp (200 mW/cm^2) (A). Variation of the TO_3 (■, □) and LO_3 (●, ○) Si–O–Si antisymmetric stretching bands (B). Full and open symbols indicate respectively the use of a 254 and 365 nm reflector.

condensation might occur by the presence of UV–C (100–280 nm) enhanced by the 254 nm reflector that was sufficient to induce electronic excitation and consumption of Si–OH groups.

Effect of Primary Parameters on Hydrolysis Kinetics. An interesting analogy can be drawn between the photoinduced sol–gel process and the moisture-induced cross-linking in alkoxy silicone and polyethylene thick films (>100 μm) used in sealants and power cables and proceeding through a similar polymerization mechanism. [29,30] Remarkably in our case, well-condensed silica films were achieved in a matter of minutes under ambient atmosphere despite conditions that might appear not optimal with a moisture-limited atmosphere (RH = 30%) and the use of nonpolar precursors converted into solid cross-linked films. The high reactivity found in our system must be analyzed by raising the combined effect of thin film conditions (≤1 μm) favorable to moisture diffusion and an efficient catalysis resulting from the photogenerated Brönsted superacids.

In sol–gel photopolymerization, the overall reaction kinetics is expected to be controlled by the two independent phenomena: the intrinsic chemical reaction rates and the water vapor permeation into the film during the hydrolysis step. Even though the development of a comprehensive model is beyond the scope of this study, their relative importance was discussed with respect to the effects of several processing parameters on the hydrolysis kinetics. First, we addressed the influence of variables affecting mainly the permeation of atmospheric water into the sol–gel matrix, such as the relative humidity and the film thickness. On the other hand, the context of reaction control would suggest a higher sensitivity to other parameters such as the exitance, the photoacid structure, and its concentration that were investigated thoroughly. No previous

dx.doi.org/10.1021/jp212386e | J. Phys. Chem. B XXXX, XXX, XXX–XXX

study is reported in the literature, where a systematic approach has been adopted to investigate the effects of various reaction primary parameters and infer the prevailing rate-controlling regime. Table 2 summarizes the effects of all these experimental parameters on hydrolysis degree and rate of PDMOS and PDEOS.

Table 2. Effect of Various Experimental Parameters on Hydrolysis Degree and Rate during the Sol−Gel Photopolymerization of PDMOS and PDEOS

		PDMOS		PDEOS	
		r_p^{rel} [a]	hydrolysis (%) t = 300 s	r_p^{rel} [a]	hydrolysis (%) t = 300 s
liquid film thickness (μm)	1.5	0.63	>95		
	2.3			0.71	>95
	0.9	1.00	>95		
	1.9			1.00	>95
	0.8	1.30	>95		
	1.4			1.12	>95
relative humidity (%)	21	0.58	>95	0.58	>95
	24	0.84	>95	0.65	>95
	30	1.00	>95	1.00	>95
	55	1.16	85		
[PAG] (wt %)	1	0.86	>95	0.64	>95
	2	1.00	>95	1.00	>95
	3	1.06	>95	1.14	>95
	4	1.03	>95	1.29	90
exitance (mW cm^{-2})	50	0.77	>95	0.33	>95
	100	1.00	>95	0.57	>95
	150	1.14	>95	0.78	>95
	200	1.00	>95	1.00	>95

[a] r_p^{rel} relative rate of hydrolysis rate, reference rate of experiment made with exitance: 200 mW/cm^2, RH: 30%, [PAG]: 2 wt %, film thickness: 0.9 μm (PDMOS) and 1.9 μm (PDEOS).

Investigation of Water Vapor Permeation. The dependency of film thickness (0.8−1.5 μm) and relative humidity (RH, 20−55%) on the hydrolysis kinetics of PDMOS films was illustrated in Figures 8A and 8B. Both figures were instrumental in proving the existence of a diffusion-controlled regime.

Although a complete hydrolysis was achieved regardless of the thickness, the first plot clearly showed a differentiation between the samples with a maximal hydrolysis rate decreasing with the film thickness. A diffusion limitation effect was evidenced with faster hydrolysis kinetics obtained with thinner films, promoting the permeation of water. Similarly, an increase of RH at constant temperature and air pressure implies a higher water vapor pressure e.[17] As expected, such conditions were suitable to the entry of water vapor into the film, affording higher initial hydrolysis rates. Nevertheless, a limiting conversion (90%) was found at the highest RH of 55%. After the first seconds of irradiation, the hydrolysis rate witnessed a sharp decrease, whereas that of the others reactions conducted at lower RH remained relatively steady. This later result reflects a solvation effect of the superacids by water molecules. In water excess, superacids are hydrolyzed leading to their replacement by H_3O^+ with a lower acidity and weaker catalytic activity. The acidity of the superacids is limited indeed by the basicity of water initially present, leading to the formation of H_3O^+ hydronium ions.

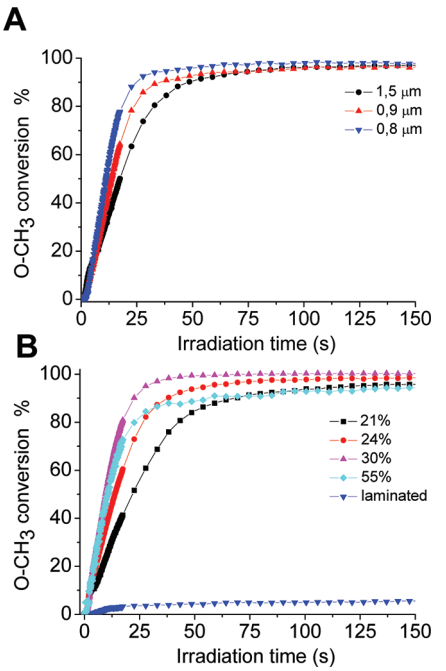

Figure 8. Methoxy conversion during the sol−gel photopolymerization of PDMOS. Influence of film thickness (A): 1.5 μm (●), 0.9 μm (▲), and 0.8 μm (■). Effect of RH (B): 21% (■), 24% (●), 30% (▲), 55% (◇). The effect of laminated conditions that prevent the entry of atmospheric moisture was also assessed (▼).

The ambient atmosphere plays the determining role of water reservoir, as proved by a simple experiment in which the permeation of water was blocked by the presence of a UV and IR transparent BaF_2 pellet placed at the top of the PDMOS film (Figure 8B). Under these conditions, hydrolysis was significantly inhibited: a slower reaction rate and a final conversion of less than 10% were obtained. The film remained liquid after 5 min of irradiation, and the water initially dissolved into the oligomeric precursor presumably accounts for the partial hydrolysis of the methoxysilyl functions. In laminated conditions, water consumed by the reaction cannot be replenished by the atmosphere, but the depletion of water initially dissolved in PDMOS (by evaporation) is also impossible. Although there are two chemical reactions in a sol−gel process, with only hydrolysis step consuming water, the final degree of condensation will also depend on water vapor permeation. Note that a similar evolution was observed with PDEOS (Table 2).

A corollary of a diffusion-controlled regime is the possible formation of a composition gradient across the z-axis. In other words, a gradual change in composition throughout the film thickness may possibly occur with the external layers being more condensed than the interior layers closer to the substrate. Owing to the submicrometric size scale of the film thickness, a nonuniform conversion is very difficult to evidence. Nevertheless, diffusion-controlled hydrolysis kinetics demonstrated previously does not necessarily imply composition gradient in the film. Combination of thin films and continued condensation due to the persistence of photoacids are likely to level the degree of condensation to a rather constant value despite apparent differences in hydrolysis kinetics.[31]

dx.doi.org/10.1021/jp212386e | J. Phys. Chem. B XXXX, XXX, XXX−XXX

A last issue is to inter-relate water sorption behavior with polymer microstructure, given that this latter is constantly evolving during the irradiation time. As displayed previously in Figure 5A, the increase in water concentration takes place in two steps bordered by the end of hydrolysis, suggesting two distinct water permeation regimes. Mass transfer of gases and vapor in dense (nonporous) films occurs mainly through the so-called activated diffusion mechanism:[32] first, water vapor condenses and dissolves into the surface; then, water migrates inward as a result of a concentration (or activity) gradient. The mechanism of liquid and vapor permeation thus involves both solution and diffusion. When penetrant flux obeys Fick's law, the permeability coefficient, P, can be expressed simply as the product of the solubility coefficient S and the diffusivity coefficient D (eq 2).

$$P = S \times D \tag{2}$$

As specific interactions (such as hydrogen bonding) between penetrant and hydrolyzed PDMOS cannot be ruled out, the relationship among P, S, and D is probably more complicated (deviation from Henry's law). In addition, the film is not in steady state since significant variations in diffusivity and solubility characteristics are expected during the reaction time with the shift from a liquid precursor to a solid cross-linked silica film. As shown in Figure 5A for PDMOS, an equilibrium water concentration has clearly difficulty to establish because the polymerization process induces film structure modification while involving consumption (hydrolysis) and formation (condensation) of water. However, eq 2 has the merit of emphasizing that penetration of water vapor will depend mainly on the relative magnitude of water solubility and diffusivity. The solubility of a penetrant depends mainly on its condensability and its interactions with the film. Diffusion coefficients, apart from their concentration dependence, are controlled by penetrant size and shape, while film crystallinity and chain mobility have also important effects on the transport process.[33,34]

At the beginning, a free chain motion is associated with the liquid alkoxy oligomer chains. Despite their hydrophobicity minimizing the solubility coefficient, siloxane chains are thought to participate in the diffusion process due to internal chain micromotions, enabling a larger amount of free volume in which diffusion may take place to ensure an efficient hydrolysis. As a result of sol–gel transition, the film becomes cross-linked and hydrophilic properties appear due to the replacement of alkoxide groups (OR) with hydroxyl groups (OH). Under these conditions, water permeation becomes controlled by the solubility characteristic and less by diffusivity because of limited chain mobility in amorphous cross-linked silica. With the formation of hydrophilic silanol, the water vapor will have an enhanced solubility parameter, close to that of the film, offsetting the loss of diffusivity related to solidification.

Investigation of Chemical Reaction Parameters. With regard to chemical reaction parameters, the concentration in PAG has been varied from 1 to 4 wt %, and the exitance of the Hg–Xe lamp has been varied from 50 to 200 mW/cm^2 (Table 2). There is no significant variation in the rate and the extent of hydrolysis in the selected range of PAG concentrations. In contrast, traditional sol–gel polymerization in water solution was most influenced by the concentration of the acid catalyst.[24,35,36] This result argues for a diffusion-controlled regime even at low PAG concentration (1%) due to the high reactivity of the UV-generated photoacids. Similarly, a decrease of the exitance which affects the PAG photolysis rate shows small effects on the hydrolysis conversion curves. In the present conditions, the rate-determining step is clearly the water permeation in the film. Though a diffusional resistance is evidenced, such result must be analyzed and be put into proper perspective since very fast hydrolysis reactions were obtained regardless of the experimental conditions chosen. In contrast, PDEOS shows a higher dependency to PAG concentration and exitance variation, suggesting a combined rate-limiting regime. As observed in sol–gel chemistry, increasing the steric hindrance of the alkoxy group is marked by lowered hydrolysis kinetics, which enhances the effect of chemical reaction parameters.[20,21]

The nature of the photoacid exerts the greatest effects on the hydrolysis kinetics: the structure of the photoacid is defined by the nature of the counterion, which is a weakly coordinating anion. Nature and stability of the anion will influence the acid strength and will be determinant for the initiation efficiency of the reaction as represented in Figure 9.

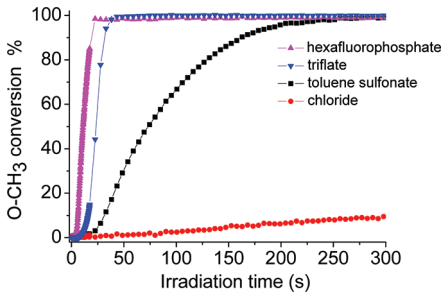

Figure 9. Methoxy conversion during the sol–gel photopolymerization of a PDMOS film containing 2% wt of PAG with different counterion: hexafluorophosphate (PF_6^-, ◆), triflate ($CF_3SO_3^-$,▲), toluenesulfonate ($CH_3\Phi SO_3^-$, ■) and chloride (Cl^-, ●).

In cationic photopolymerization of epoxy or vinyl ether monomers, a larger charge delocalization of the anion confers generally a stronger acidity and implies a higher catalytic efficiency.[2] Thus, the reactivity order observed is generally hexafluorophosphate (PF_6^-) > triflate ($CF_3SO_3^-$) > toluenesulfonate ($CH_3\Phi SO_3^-$) ≫ chloride (Cl^-). Thus, important variations were observed in the hydrolysis conversion plots depending on the nature of the counterion represented in Figure 9. Although a full consumption of the methoxysilyl groups was reported with hexafluorophosphate, triflate, and toluene sulfonate as counterions, a retarding effect of the lower acid catalyst is clearly evident. In the case of H^+Cl^-, only 10% conversion was obtained. This is not only the result of a decreased catalyst activity with the low nucleophilic chloride anion, evaporation of hydrochloric acid in thin film precursor possibly accounts for this result. Other photoacid possessing bulkier anions are less likely to evaporate. It should be noted finally that with a decrease of the photocatalyst reactivity the system is likely to become reaction rate control.

CONCLUSION

RT-FTIR represents a complete and comprehensive technique to study the photoacid-catalyzed sol–gel polymerization *in situ*. A full picture of this inorganic photopolymerization mechanism has been provided, from hydrolysis to condensation kinetics, as well as an insight into the fate of water and alcohol byproducts. Concerning the driving forces of this reaction, it has been

dx.doi.org/10.1021/jp212386e | J. Phys. Chem. B XXXX, XXX, XXX–XXX

established that, in addition to a catalytic effect by the photogenerated Brönsted acids, the energetic photons (UVC) are responsible for a direct densification through electronic excitation of silanol groups and siloxane bonds. The occurrence of a water permeation controlled-regime was demonstrated with the methoxy precursor (PDMOS), whereas its ethoxy analogue shows a combined regime dependent also on the intrinsic chemical reaction parameters (exitance, PAG nature, and concentration).

Fast hydrolysis rates and the elimination of organic solvent (and even water) are major features of sol−gel photopolymerization compared with conventional sol−gel methodologies. This should help to revisit, and possibly simplify, the synthesis of many sol−gel materials including hybrid, nanostructured, and mesoporous films. Second, spatially directed UV irradiation is an opportunity to create novel materials not accessible by traditional sol−gel chemistry and applicable in emerging technologies, including microfluidics, photonics, and membrane.

■ ASSOCIATED CONTENT

Ⓢ Supporting Information

^{29}Si liquid state NMR spectra of PDMOS and PDEOS (Figures S1 and S2); emission spectra of the Hg−Xe lamp with a reflector at 365 and 254 nm (Figure S3). This material is available free of charge via the Internet at http://pubs.acs.org.

■ AUTHOR INFORMATION

Corresponding Author

*E-mail abraham.chemtob@uha.fr; Tel +33 3 8933 5030; Fax +33 3 8933 5017.

Notes

The authors declare no competing financial interest.

■ REFERENCES

(1) Fox, F. J.; Noren, R. W.; Krankkala, G. E. US Patent 4,101,513, 1978.
(2) Crivello, J. V. *J. Polym. Sci., Part A* **1999**, *37*, 4241−4254.
(3) Kowalewska, A. *J. Mater. Chem.* **2005**, *15*, 4997−5006.
(4) Amerio, E.; Sangermano, M.; Malucelli, G.; Priola, A.; Voit, B. *Polymer* **2005**, *46*, 11241−11246.
(5) Chemtob, A.; Versace, D.-L.; Belon, C.; Croutxe-Barghorn, C.; Rigolet, S. *Macromolecules* **2008**, *41*, 7390−7398.
(6) Sallenave, X.; Dautel, O. J.; Wantz, G.; Valvin, P.; Lère-Porte, J.-P.; Moreau, J. J. E. *Adv. Funct. Mater.* **2009**, *19*, 404−410.
(7) Chemtob, A.; Belon, C.; Croutxe-Barghorn, C.; Brendle, J.; Soulard, M.; Rigolet, S.; Le Houerou, V.; Gauthier, C. *New J. Chem.* **2010**, *34*, 1068−1072.
(8) Galeener, F. L. *Phys. Rev. B* **1979**, *19*, 4292−4297.
(9) Matos, M. C.; Ilharco, L. M.; Almeida, R. M. *J. Non-Cryst. Solids* **1992**, *147−148*, 232−237.
(10) Niznansky, D.; Rehspringer, J. L. *J. Non-Cryst. Solids* **1995**, *180*, 191−196.
(11) Rubio, F.; Rubio, J.; Oteo, J. L. *Spectrosc. Lett.* **1998**, *31*, 199−219.
(12) Fidalgo, A.; Ilharco, L. *J. Non-Cryst. Solids* **2001**, *283*, 144−154.
(13) Innocenzi, P. *J. Non-Cryst. Solids* **2003**, *316*, 309−319.
(14) Falcaro, P.; Costacurta, S.; Mattei, G.; Amenitsch, H.; Marcelli, A.; Guidi, M. C.; Piccinini, M.; Nucara, A.; Malfatti, L.; Kidchob.; et al. *J. Am. Chem. Soc.* **2005**, *127*, 3838−3846.
(15) Innocenzi, P.; Kidchob, T.; Bertolo, J.; Piccinini, M.; Guidi, M.; Marcelli, C. *J. Phys. Chem. B* **2006**, *110*, 10837−10841.
(16) Doshi, D.; Gibaud, A.; Goletto, V.; Mengcheng, L.; Gerung, H.; Ocko, B.; Han, S.; Brinker, C. *J. Am. Chem. Soc.* **2003**, *125*, 11646−11655.
(17) The RH with respect to water is the ratio (expressed as a percentage) of the actual pressure *e* due to water vapor pressure in air and *es* the saturation vapor pressure. *es* is also referred to as equilibrium vapor pressure as it corresponds to the pressure exerted by water vapor in equilibrium with a plane surface of pure water.
(18) Massiot, D.; Fayon, F.; Capron, M.; King, I.; Le Calvé, S.; Alonso, B.; Durand, J.-O.; Bujoli, B.; Gan, Z.; Hoatson, G. *Magn. Reson. Chem.* **2002**, *40*, 70−76.
(19) There are other vibrational modes of silica arising in the lower frequency region at 460 and 800 cm^{-1} assigned to Si−O−Si rocking (TO_1) and symmetric stretching (TO_2), respectively, which are of little interest in our case. TO_1 is obstructed by the absorption of the substrate (BaF_2) while the TO_2 is broad with significant overlap with the symmetric stretching of the (Si)−O−C bands at 839 cm^{-1}.
(20) Judeinstein, P.; Sanchez, C. *J. Mater. Chem.* **1996**, *6*, 511−525.
(21) Loy, D.; Baugher, B.; Baugher, C.; Schneider, D.; Rahimian, K. *Chem. Mater.* **2000**, *12*, 3624−3632.
(22) Vega, A.; Scherer, G. *J. Non-Cryst. Solids* **1989**, *111*, 153−166.
(23) Trzpit, M.; Rigolet, S.; Paillaud, J.-L.; Marichal, C.; Soulard, M.; Patarin, J. *J. Phys. Chem. B* **2008**, *112*, 7257−7266.
(24) Brinker, C.; Scherer, G. *Sol-Gel Science: The Physics and Chemistry of Sol Gel Processing*; Academic Press: San Diego, 1990.
(25) Maekawa, S.; Ohishi, T. *J. Non-Cryst. Solids* **1994**, *169*, 207−209.
(26) Imai, H.; Awazu, K.; Yasumori, M.; Onuki, H.; Hirashima, H. *J. Sol-Gel Sci. Technol.* **1997**, *8*, 365−369.
(27) Tsuzuki, Y.; Oikubo, Y.; Matsuura, Y.; Itatani, K.; Koda, S. *J. Sol-Gel Sci. Technol.* **2008**, *47*, 131−139.
(28) Imai, H.; Yasumori, M.; Hirashima, H.; Awazu, K.; Onuki, H. *J. Appl. Phys.* **1996**, *79*, 8304−8309.
(29) Gosh-Dastidar, A.; Sengupta, S. S.; Cogen, J. M.; Gross, L. H.; Shurott, S. F. *Int. Wire Cable Symp.* **2007**, *56*, 436−442.
(30) Comyn, J.; de Buyl, F.; Shephard, N. E.; Subramaniam, C. *Int. J. Adhes. Adhes.* **2002**, *22*, 385−393.
(31) Note: it is also worth mentioning that a gradient composition can also arise from the inhomogeneity of UV irradiation with a light penetrating no uniformly throughout the entire volume. In our case, the low absorption wavelength of diphenyliodonium salts (λ_{max} 227 nm) implies a homogeneous light penetration by the Hg−Xe lamp (250−390 nm).
(32) Viet, W. R. Hanser: Munich, 1991.
(33) Merkel, T. C.; Bondar, V. I.; Nagai, K.; Freeman, B. D.; Pinnau, I. *J. Polym. Sci., Part B* **2000**, *38*, 415−434.
(34) Lin, H.; Kai, T.; Freeman, B. D.; Kalakkunnath, S.; Kalika, D. S. *Macromolecules* **2005**, *38*, 8381−8393.
(35) Aelion, R.; Loebel, A.; Eirich, F. *J. Am. Chem. Soc.* **1950**, *72*, 5705−5712.
(36) Pope, E. J. A.; Mackenzie, J. D. *J. Non-Cryst. Solids* **1986**, *87*, 185−198.